


Article

Development of Grid-Forming and Grid-Following Inverter Control in Microgrid Network Ensuring Grid Stability and Frequency Response

V. Vignesh Babu ¹, J. Preetha Roselyn ^{1,*}, C. Nithya ¹ and Prabha Sundaravadivel ^{2,*} 

¹ Department of EEE, SRM Institute of Science and Technology, Kattankulathur, Chennai 603203, Tamil Nadu, India; ve.vigneshme@gmail.com (V.V.B.); nithyac@srmist.edu.in (C.N.)

² Department of Electrical and Computer Engineering, The University of Texas at Tyler, Tyler, TX 75701, USA

* Correspondence: preethaj@srmist.edu.in (J.P.R.); psundaravadivel@uttyler.edu (P.S.)

Abstract: This paper proposes a control strategy for grid-following inverter control and grid-forming inverter control developed for a Solar Photovoltaic (PV)–battery-integrated microgrid network. A grid-following (GFL) inverter with real and reactive power control in a solar PV-fed system is developed; it uses a Phase Lock Loop (PLL) to track the phase angle of the voltages at the PCC and adopts a vector control strategy to adjust the active and reactive currents that are injected into the power grid. The drawback of a GFL inverter is that it lacks the capability to operate independently when the utility grid is down due to outages or disturbances. The proposed grid-forming (GFM) inverter control with a virtual synchronous machine provides inertia to the grid, generates a stable grid-like voltage and frequency and enables the integration of the grid. The proposed system incorporates a battery energy storage system (BESS) which has inherent energy storage capability and is independent of geographical areas. The GFM control includes voltage and frequency control, enhanced islanding and black start capability and the maintenance of the stability of the grid-integrated system. The proposed model is validated under varying irradiance conditions, load switching, grid outages and temporary faults with fault ride-through (FRT) capability, and fast frequency response and stability are achieved. The proposed model is validated under varying irradiance conditions, load switching, grid outages and line faults incorporating fault ride-through capability in GFM-based control. The proposed controller was simulated in a 100 MW solar PV system and 60 MW BESS using the MATLAB/Simulink 2023 tool, and the experimental setup was validated in a 1 kW grid-connected system. The percentage improvement of the system frequency and voltage with FRT-capable GFM control is 69.3% and 70%, respectively, and the percentage improvement is only 3% for system frequency and 52% for grid voltage in the case of an FRT-capable GFL controller. The simulation and experimental results prove that GFM-based inverter control achieves fast frequency response, and grid stability is also ensured.

Keywords: grid-forming inverter; grid-following inverter; fault ride-through capability; microgrid; photovoltaic energy; power electronics



Citation: Babu, V.V.; Roselyn, J.P.; Nithya, C.; Sundaravadivel, P. Development of Grid-Forming and Grid-Following Inverter Control in Microgrid Network Ensuring Grid Stability and Frequency Response. *Electronics* **2024**, *13*, 1958. <https://doi.org/10.3390/electronics13101958>

Academic Editors: Vincenzo d'Alessandro, Antonio Pio Catalano and Ciro Scognamiglio

Received: 16 April 2024

Revised: 9 May 2024

Accepted: 14 May 2024

Published: 16 May 2024



Copyright: © 2024 by the authors. Licensee MDPI, Basel, Switzerland. This article is an open access article distributed under the terms and conditions of the Creative Commons Attribution (CC BY) license (<https://creativecommons.org/licenses/by/4.0/>).

1. Introduction

The power system is experiencing stability issues due to the increased penetration of inverter-based renewable resources (IBRs) due to a drastic reduction in system inertia [1,2]. IBRs are replacing the generation of power from synchronous generators in the power system due to the increased penetration of renewable energy sources. This leads to reduced synchronization torque, less inertia and limitations on short circuit current, which become challenges in IBR-dominated power systems [3]. In addition, the intermittent variations of renewable power generation create fluctuations in the voltage and frequency of the power system. The challenges of IBR-dominated power systems are as follows: (a) the impact of degrading grid strength and short circuit current levels on stability and adequacy

of protection; (b) degrading system inertia impacts on power system stability; (c) grid formation in the absence of synchronous generators and islanded mode of operation; (d) jump-starting the grid after blackouts.

There are two types of inverters by which renewables are integrated into the grid for injection of renewable power, namely grid-following (GFL) inverters and grid-forming (GFM) inverters. Most grid-connected renewables in the last decade have operated with the GFL type of inverter which is dependent on external grid set points, and due to communication delays, a fast response from a GFL inverter is not possible for any system changes [4]. As IBR penetration increases, the controllers of inverters must respond more robustly to a system with faster dynamics and enhance the inverter capability to support the power system stability [5–10]. A GFL inverter acts as a current source and follows the grid voltage with proper synchronization. In addition, GFL inverters cannot provide inertia to the system, and hence, the dynamic behavior of a synchronous generator is not mimicked for the effect of inertia in the power system. Unlike synchronous generators, which adapt to variations in grid frequency, GFL inverters normally operate at their rated output power [11]. The GFL control must be synchronized to the grid using a phase-locked loop (PLL) which provides a phase angle and frequency to synchronize the renewable-fed inverter to the grid [12]. GFL consists of two control loops, namely the slower voltage control loop and the faster inner current control loop [13]. The GFL inverter is not able to regulate the voltage and frequency of the system directly and hence cannot operate when voltage or frequency instability occurs in the power system. Hence, in recent years, researchers have developed the concept of a grid-forming inverter for IBRs. IBRs with GFM control are capable of supporting the grid during normal and fault conditions, including islanding situations, by behaving as voltage sources with specified voltage magnitude, phase angle and frequency. The desirable functionalities of the GFM-based IBRs are as follows: (a) GFM control works faster than GFL control to maintain voltage and frequency; (b) system stability contribution; (c) provision of synchronizing and damping torque; (d) lower rate of change of frequency and black start capability.

As maintaining the synchronous generation online during grid failure and grid islanding is expensive and difficult, energy storage systems have provided a better alternative solution. Many articles have focused on the development of controllers for GFL inverters, and GFM inverters have received increased attention in recent years. In [14], a droop-controlled GFM inverter is compared against a frequency-support-based GFL inverter. The system performance is analyzed at different penetration levels of renewables and various inertia levels of the system. The frequency-controlled GFL inverter results in reduced damping and higher frequency excursion. But for the system with a GFM inverter, the frequency damping is increased and smoothly transfers the overloading to the other sources, hence maintaining the reliability of the system.

The performance of GFL and GFM inverters in a low-inertia dynamic model with a BESS is presented in [15], which gives a comparison between the various case studies. The results allowed the conclusion that GFM control outperforms GFL control in terms of system frequency. In [16], the authors proposed the duality between GFM and GFL inverters with respect to synchronization loop, grid interfacing characteristics, swing characteristics, control gain characteristics, grid strength compatibility and transient stability. The investigation in [17] made it clear that the voltage control function may lessen voltage fluctuations following fault, improving the active power response of virtual inertia GFL. Virtual synchronous generators is a concept proposed in [18] for stabilizing frequency fluctuations on grids with IBR dominance. A simulation-based analysis of a GFM power inverter controller is performed in [19] to better understand voltage and frequency stabilization, as well as to ensure that critical electrical loads are not affected during prolonged power outages. The review paper [20] examines droop-based GFM inverters, virtual synchronous generator (VSG)-based GFM inverters, compensated generalized VSG (CGVSG)-based GFM inverters and adaptive VSG (AVSG)-based GFM inverters. Various operational scenarios are compared in terms of their performance and robustness in the

article. In [21], a power converter for PV systems is investigated during system faults. GFM inverters are being used in microgrid projects in a variety of topologies and configurations. However, several challenges need to be addressed before synchronous machines can be replaced by GFM inverters at the transmission level. Developing hardware, software and controls for network models; standardizing inverter models; integrating renewable energy sources into the system; energy storage; stability analysis; networking capabilities for black starts; dynamic islanding topology solutions; and economic dispatch are some of these challenges and research gaps identified with respect to grid-forming inverters connected to microgrids [22–26].

The voltage control function has the ability to reduce the eigen oscillation among synchronous generators. In terms of system frequency stability, the virtual inertia GFL control did well in raising the nadir to the same level as the virtual inertia GFM control, but it was unable to raise the rate of change of frequency (RoCoF) by the same amount. During frequency disturbance, a GFM-based inverter can provide an instantaneous response without any external measurements, whereas a GFL-based inverter experiences a delay of ten to hundreds of milliseconds. The dependency of the PLL in GFL-based inverters in reacting to system disturbances in a low-inertia system makes the system weak due to the loss of synchronism during disturbances, which can be overcome by GFM inverters by reducing the rate of change of frequency and frequency deviation. GFM control also supports the voltage stability of the system following a disturbance. There is the additional support of the capability to damp the power oscillations in both sub-synchronous and super-synchronous modes. The black start capability of the GFM inverter supporting restoration processes makes the controller more attractive in a power system. Based on the literature study, it is understood that the study of the transient response of GFM-based inverter control during system disturbances is very critical, and hence, control should improve the dynamic capability of GFM control. The enhancement of grid synchronization of the proposed inverter control is essential without external grid support. Proper control strategies are required to provide plug-and-play operations of renewable energy integration into the system in GFM-based inverters. FRT-capable inverter control is essential for sustaining the system under fault conditions.

The main contributions of this paper are as follows:

- The proposed IBR control strategy consists of two control operations in a renewable-fed inverter, namely grid-following control and grid-forming control.
- A virtual synchronous machine (VSM)-based GFM inverter control is developed to regulate the voltage and frequency of the power system along with active power control and reactive power control which significantly improve the dynamic performance of the grid-connected microgrid network.
- Two methods of PLLs are used for synchronization: phase-locked loop for obtaining the phase voltage at the PCC, and power balance synchronization, to regulate the frequency.
- The proposed inverter control strategy is developed and implemented in a simulation environment of a 1 kW grid-connected microgrid system and the hardware setup of a 100 kW microgrid network.
- The proposed control strategies are tested under different system conditions like varying irradiation, varying demand conditions and fault conditions.

The organization of the paper is as follows: The proposed framework of coordinated control of GFL and GFM inverters in an inverter-fed solar PV-BESS tied with a utility grid is explained in Section 2. The description of the simulation test system and hardware setup is provided in Section 3, and Section 4 provides the simulation results and experimental results of the microgrid network. Section 5 concludes the paper and provides the scope for future work.

(a) GFL-based inverter control for Solar PV:

The grid-following-based inverter control consists of a phase-locked loop and inner current control loop for providing the control for the inverter currents as shown in Figure 3. This work utilizes active–reactive power control (PQ control) in the outer control loop. The GFL-based control in the solar PV system needs voltage measurement for acquiring the grid voltage. In GFL-based inverter control, the synchronization and reference waveform are provided by the PLL loop by which the angle of the grid voltage, θ , is determined. In this control strategy, the outer loop is used to regulate the active and reactive power injected into the grid, while the inner current is used to adjust the converter currents according to the reference values set by the outer power loop. In this work, low-voltage ride-through capability is also incorporated into the GFL inverter-fed PV system. This control technique is activated during the low-voltage conditions that occur due to system faults. This ensures stability to the power system even during system faults by injecting sufficient reactive power into the grid.

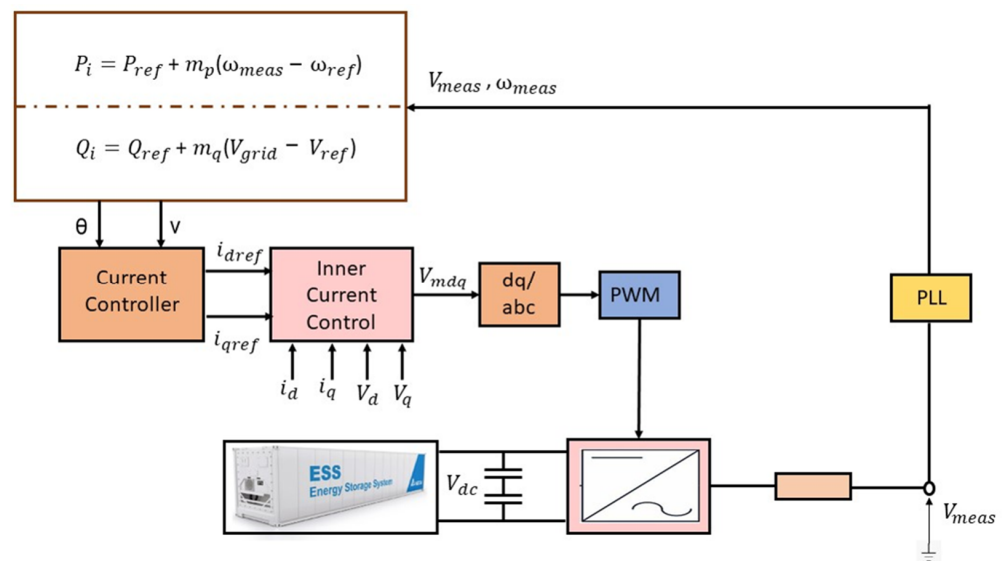


Figure 3. Flow diagram of GFL-based inverter control.

The block diagram representation of GFL-based inverter control is shown in Figure 4. The measured voltage and frequency of the grid side are fed as inputs to the GFL-based inverter control algorithm. The control inputs to the model are real and reactive power references, voltage references and frequency references. The real power, reactive power and their corresponding reference currents are estimated as follows [21]:

$$P_{ref}^* = P_{ref} + m_p (\omega_{ref} - \omega_{meas}) \quad (1)$$

$$Q_{ref}^* = Q_{ref} + m_q (V_{ref} - V_{grid}) \quad (2)$$

$$i_{dref} = \frac{P_{ref}^*}{V_{grid}} \quad (3)$$

$$i_{qref} = \frac{Q_{ref}^*}{V_{grid}} \quad (4)$$

In GFL-based inverter control, the speed of response is very limited because of the measurement delay and control delays which overall create considerable delay in the response of 10–100 ms when compared with GFM-based inverter control.

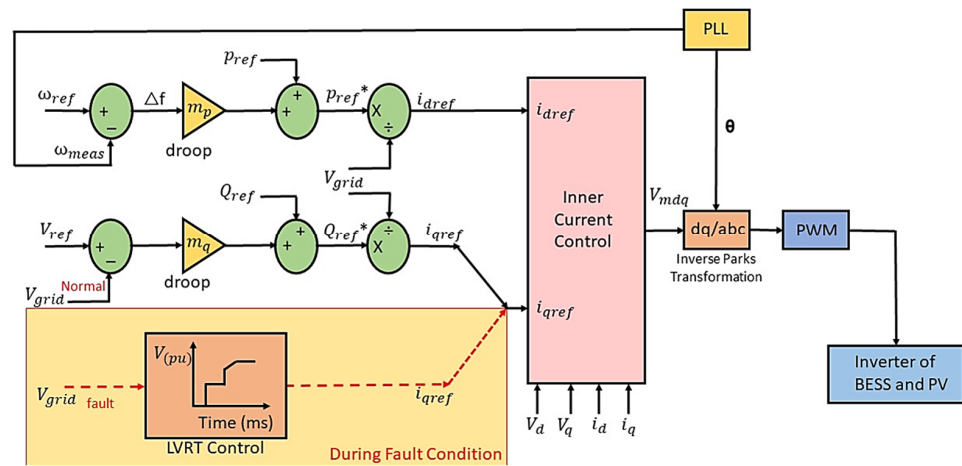


Figure 4. GFL-based inverter control for solar PV system.

(b) Virtual synchronous machine-based grid-forming inverter control for BESS:

The grid-forming-based inverter control consists of a virtual synchronous machine (VSM) for regulating the voltage and frequency of the power system along with active power control and reactive power control for significantly improving the dynamic performance of the grid-connected PV system. In this work, GFM-based inverter control is deployed for the energy storage system as mentioned in flow diagram of Figure 5. The VSM-based inverter control offers an alternative grid-synchronization method as it mimics the performance of synchronous machines which inherently synchronize to the grid, and it largely takes part in the stabilization of the grid frequency during system dynamics. The proposed model of a virtual synchronous machine can be operated in grid-connected mode and islanded mode of operation as depicted in Figure 6. The VSM are based on the measurements of the local quantities and do not depend on the external quantities as in case of the conventional synchronous machine. Further, the inertial characteristics of the VSM can provide frequency support and enhance the power sharing capability during dynamic conditions. The synchronous machine can be modeled using a swing equation to note its dominant behavior. As a key difference of the VSM, it is worth mentioning that the VSM does not depend on the tracking of reference currents or voltages. This inverter control algorithm with added virtual inertia, called virtual SGs, can contribute to the short-term stabilization of the grid frequency.

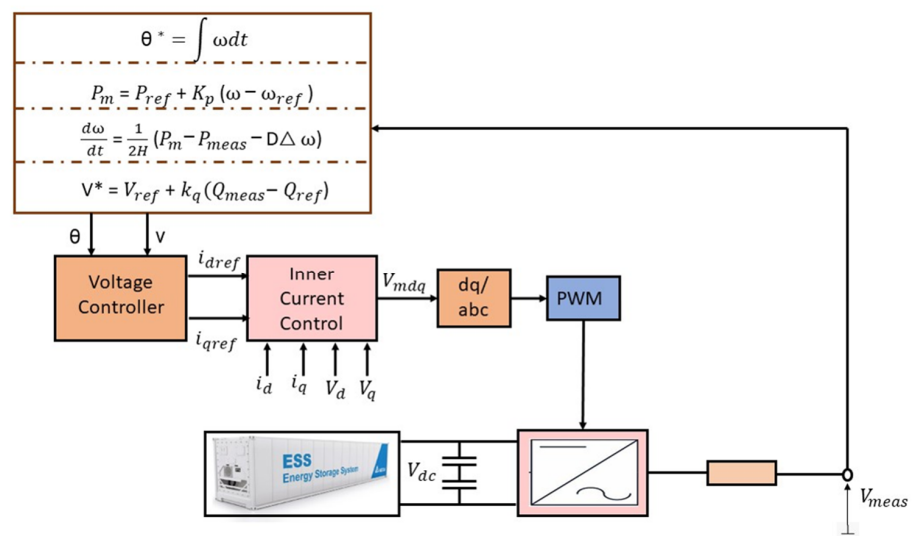


Figure 5. Flow diagram of GFM inverter control.

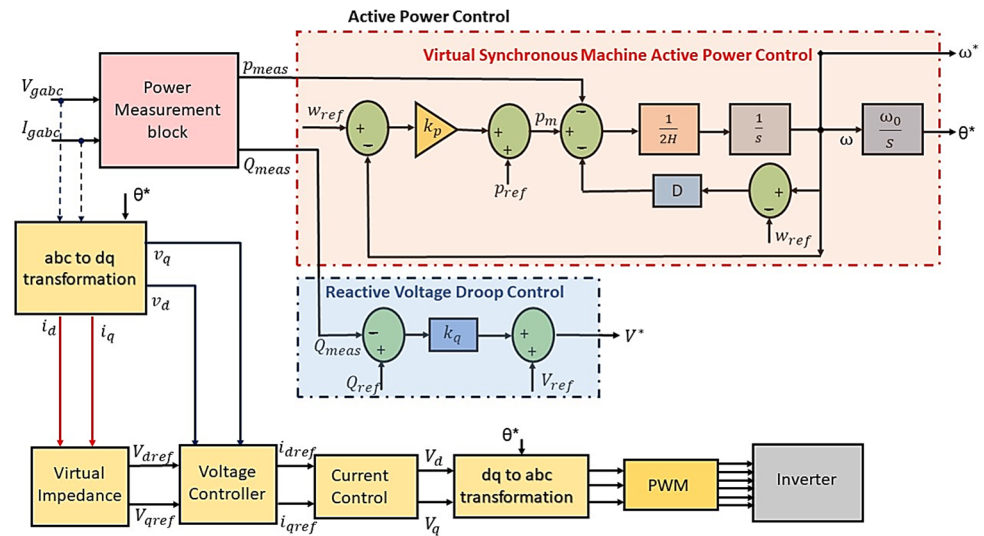


Figure 6. GFM-based inverter control for BESS.

The active power is controlled using the VSM strategy by generating the reference phase angle of the voltage for the inverter in the BESS as shown in Figure 6. The control algorithm has two variables, phase angle (θ) and frequency (ω), that are used to generate the state space equations required for the controller. The swing equation of the VSM is as shown in Equations (5)–(7) [17,18], where ω_{ref} is the reference frequency, P_{meas} is the active power generated by the inverter, P_{ref} is the reference power and P_m is the mechanical power output. The active power is controlled using a VSM-based inverter control strategy by generating the reference phase angle of the voltage for the inverter of the BESS.

$$\theta^* = \int \omega dt \quad (5)$$

$$P_m = P_{ref} - K_p(\omega - \omega_{ref}) \quad (6)$$

$$\frac{d\omega}{dt} = \frac{1}{2H}(P_m - P_{meas} - D\Delta\omega) \quad (7)$$

Droop control for the reactive power is used to achieve the voltage control of the inverter by setting the voltage magnitude of the reference voltage for the BESS as shown in Equation (8).

$$V_d = V_{ref} + k_p(Q_e - Q_{ref}) \quad (8)$$

where V_{ref} and Q_{ref} are the voltage and reactive power references of the droop controller and Q_e is the reactive power output of the BESS inverter.

The BESS is employed for high-frequency curtailment and stabilizes the system following a system fault. However, the BESS control strategy for curtailing the frequency in a grid with low inertia has been designed such that it is capable of working effectively during uncertainties and grid fault conditions.

(c) PLL-based grid synchronization:

The synchronization of the grid is maintained by regulating the terminal voltage of the PV inverter such that it matches the phase voltage, amplitude and frequency as defined by IEEE 1547-2018 [7]. In this work, two methods of PLLs are used for synchronization: a phase-locked loop for obtaining the phase voltage at the PCC and power balance synchronization, to regulate the frequency as shown in Figure 7. The phase detector block will output a signal that is proportional to the phase difference between the reference voltage and voltage generated by the internal oscillator of the PLL. The loop filter block is usually made up of a first-order low-pass filter or PI controller which will attenuate the high-frequency

components of the signal output of the previous block. The voltage-controlled oscillator generates an AC signal whose phase is compared with the input signal of the phase detector block, and the phases are matched by adjustments made to the oscillator.

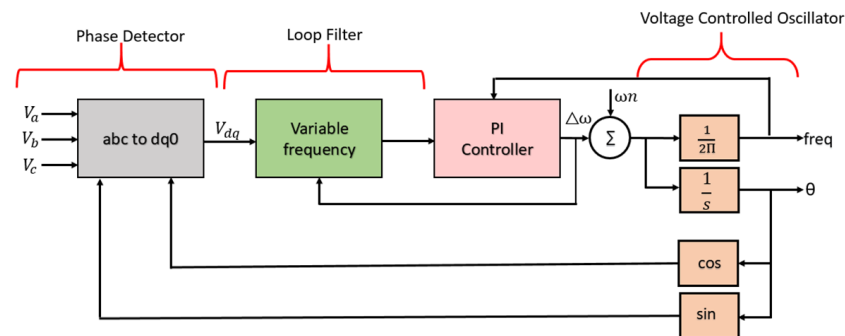


Figure 7. PLL-based grid synchronization.

3. Description of Test System

The grid-connected PV-BESS microgrid network consists of two three-phase central inverters for solar PV and energy storage systems. The PV inverter can deliver 100 MW of maximum power at a temperature of 25 °C and irradiance of 1000 W/m², and the BESS consists of a battery unit with 60 MWh capacity. The PV inverters are connected to a medium-voltage power network through a 4 kV/24.9 kV distribution transformer. The single-line diagram of the test system is shown in Figure 8. The PV array is forced to operate at its maximum power point by regulating the dc link voltage to its reference value.

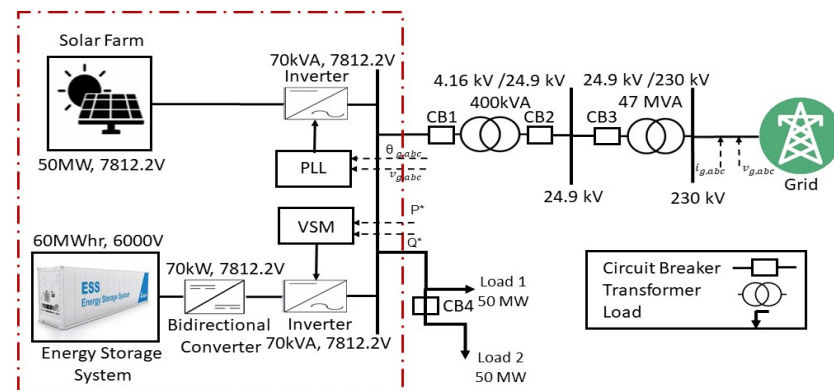


Figure 8. Single-line diagram of simulation test system.

The BESS is connected to the grid-connected PV system through a two-stage power conversion process, and the specifications of the test system are provided in Table 1.

Table 1. Specifications of simulation test system.

Parameters	Component Ratings
PV Module	100 MW
PV-Fed Inverter	120 MVA, 7 kV
Battery	60 MWh
Bidirectional Converter	70 MW, 7 kV
Battery-Fed Inverter	70 MVA, 7 kV

4. Discussion of Simulation Results

The system parameters are analyzed during normal and abnormal conditions such as load curtailment, grid outage, solar PV power variation, and temporary and permanent faults. The proposed controllers are designed based on the recommendations of IEEE standard 2800 [27]. During the ride-through period, the proposed controller generates the reference current for the PV inverter. The test system is deployed with the proposed coordinated grid-following inverter control for solar PV and grid-forming inverter control for energy storage systems. The performance of the inverter control in the energy storage side is validated by comparing the performance of the grid-following and grid-forming inverter control algorithms under different case studies.

Case 1: Variation in solar PV penetration under grid-connected mode:

The performance of the system is investigated by comparing the performance of GFM and GFL controls in the inverter side of the BESS and solar PV system, respectively. When there is a dynamic variation in solar irradiation, the system parameters are disturbed, deteriorating the stability of the system. The developed model is tested with inverter controls under GFL- and GFM-based control algorithms in the BESS side, and the results are provided in Figure 9. The voltage at PCC is stabilized at 0.99 pu in a response time of 300 ms. It is clear that the frequency of the system becomes stabilized in 300 ms with reduced switching transients in GFM inverter control. It is observed that the BESS with GFM control responds more effectively during disturbances than that with the GFL algorithm by providing inertial power, making the system obtain a quick response under varying solar irradiances. Hence, it is clear that the GFM inverter control reduces the transients during the switching period, and the values are within the nominal limits. Figure 10 displays the rate of change of frequency (RoCoF) of the different inverter control algorithms. Table 2 provides the system performance of the proposed controllers under varying levels of PV penetration in the simulation test system. The GFM-based inverter control for a BESS, when compared to GFL control, provides high inertial response capability which reduces the rate of change of frequency.

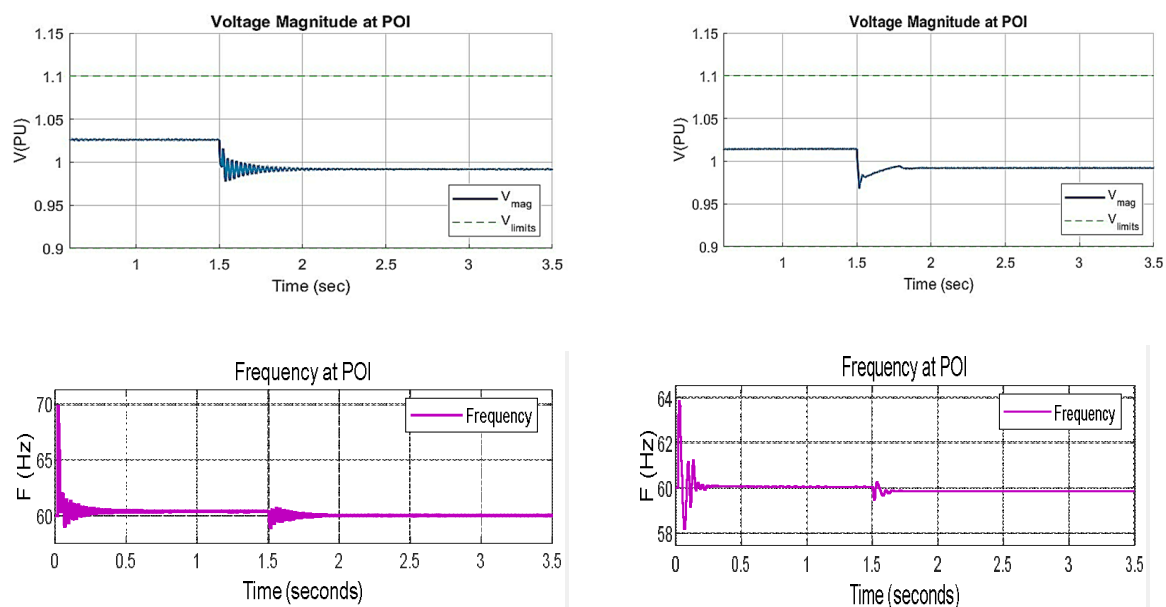


Figure 9. Cont.

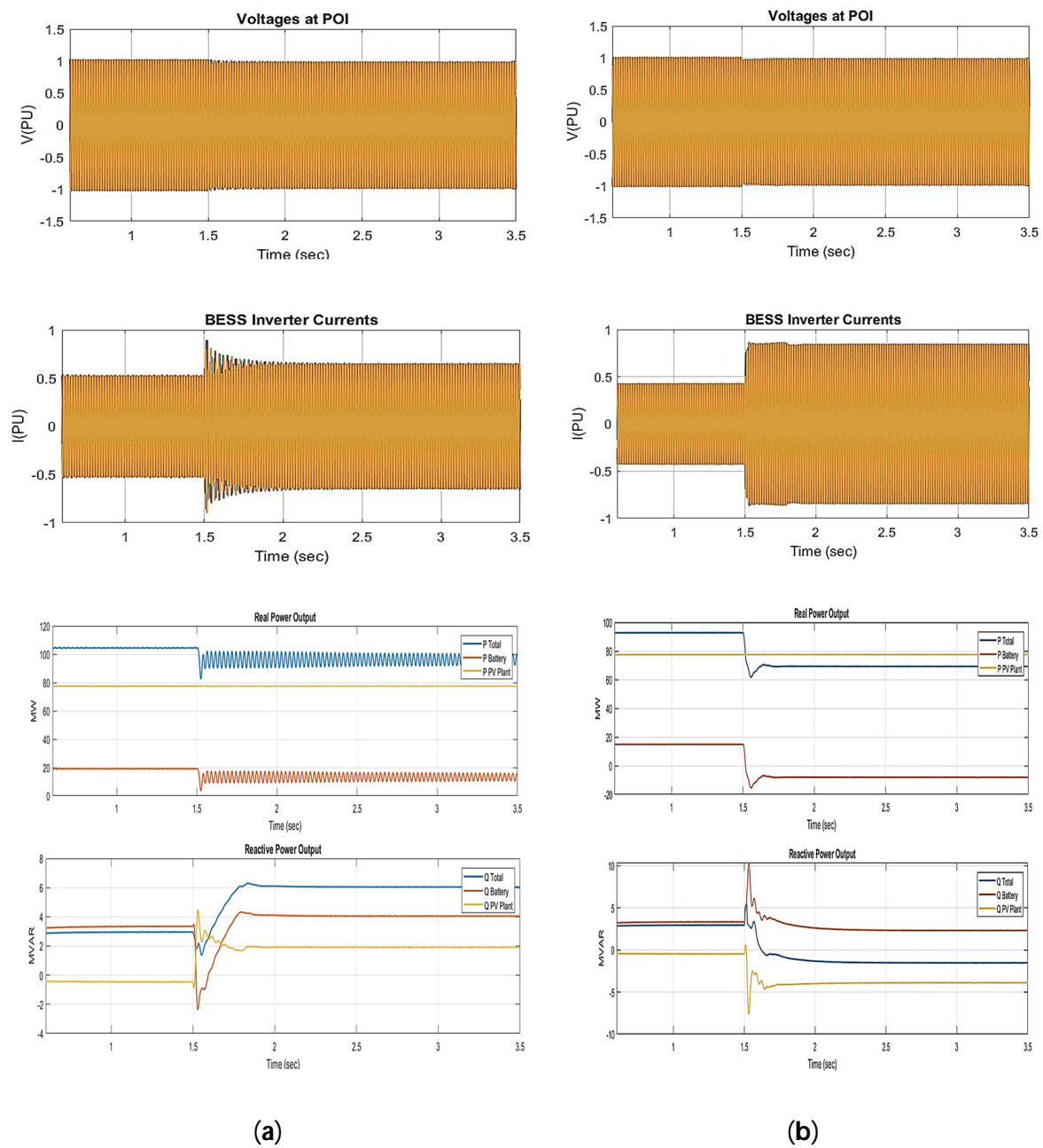


Figure 9. Performance of the system under (a) GFL and (b) GFM-based inverter control.

Table 2. System parameters under varying solar irradiation levels.

Parameters	Value	Switching Response (ms)
Voltage at PCC	0.99 pu	300
Frequency	59.75 Hz	300
Active power	76 MW	200
RoCoF	0.55 Hz	1.7 s
Reactive power	2 MVAR	300

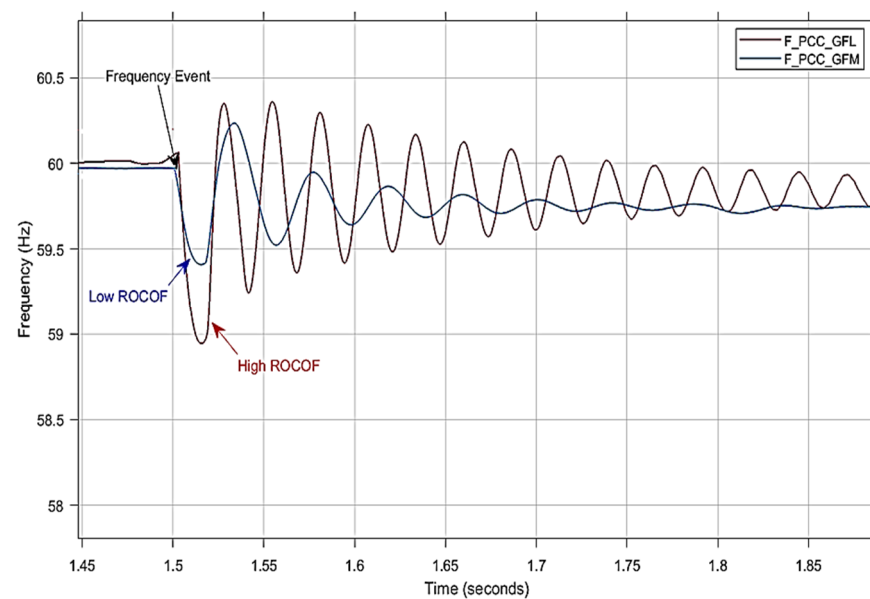


Figure 10. RoCoF comparison for GFL- and GFM-based inverter control.

Case 2: Performance of the system under varying demand conditions in a grid-connected system:

The performance of the system is tested under varying load-switching operations in a power network. The responses of the BESS-fed inverter unit under GFL and GFM control are compared for a sudden increase in the medium voltage demand as depicted in Figure 11. From the figure, it is observed that the BESS-fed inverter with the GFM control algorithm responded much faster to an increase in load and delivered the required real and reactive powers to maintain stable operation. The voltage and frequency are stabilized in a time frame of 100 and 200 ms, respectively. Table 3 depicts the performance of the coordinated GFM- and GFL-based inverter control for the grid-connected system under varying demand conditions. The GFM control regulates the active power in the prescribed range of 70% as per IEEE standard.

Case 3: Grid outages leading to islanded mode of operation:

In this case, a three-phase fault is created on the grid side at 1.5 s, and the response of the BESS with a GFM inverter during a grid outage in an islanded mode of operation is shown in Figure 12. From the simulation analysis, it is observed that the BESS with GFM control is able to deliver the required power to satisfy the medium voltage load in an islanded mode with a very fast response of 60 ms, with voltage and frequency within the acceptable limits recommended by IEEE standards. During system faults, the system parameters settle down in a shorter period for the GFM-based inverter control than the GFL control, and switching transients are much reduced in the GFM-based control system. In an islanded mode, as the BESS is connected, it provides good frequency regulation for the microgrid network. When there is a grid outage, we can observe that the BESS with GFM control can proceed to deliver the power needed by the load and run the network in an island mode with acceptable system voltage and frequency. Table 4 provides the system parameters during grid outages, and we can observe that the voltage at PCC is 1.02 per unit, and the frequency is 59.8 Hz. Table 4 depicts the performance of the coordinated GFM- and GFL-based inverter control for an islanded mode of operation due to grid outages. As the GFM-based inverter control can generate voltage and frequency without a grid in islanded operation, it is the most suitable control method for weak grid networks.

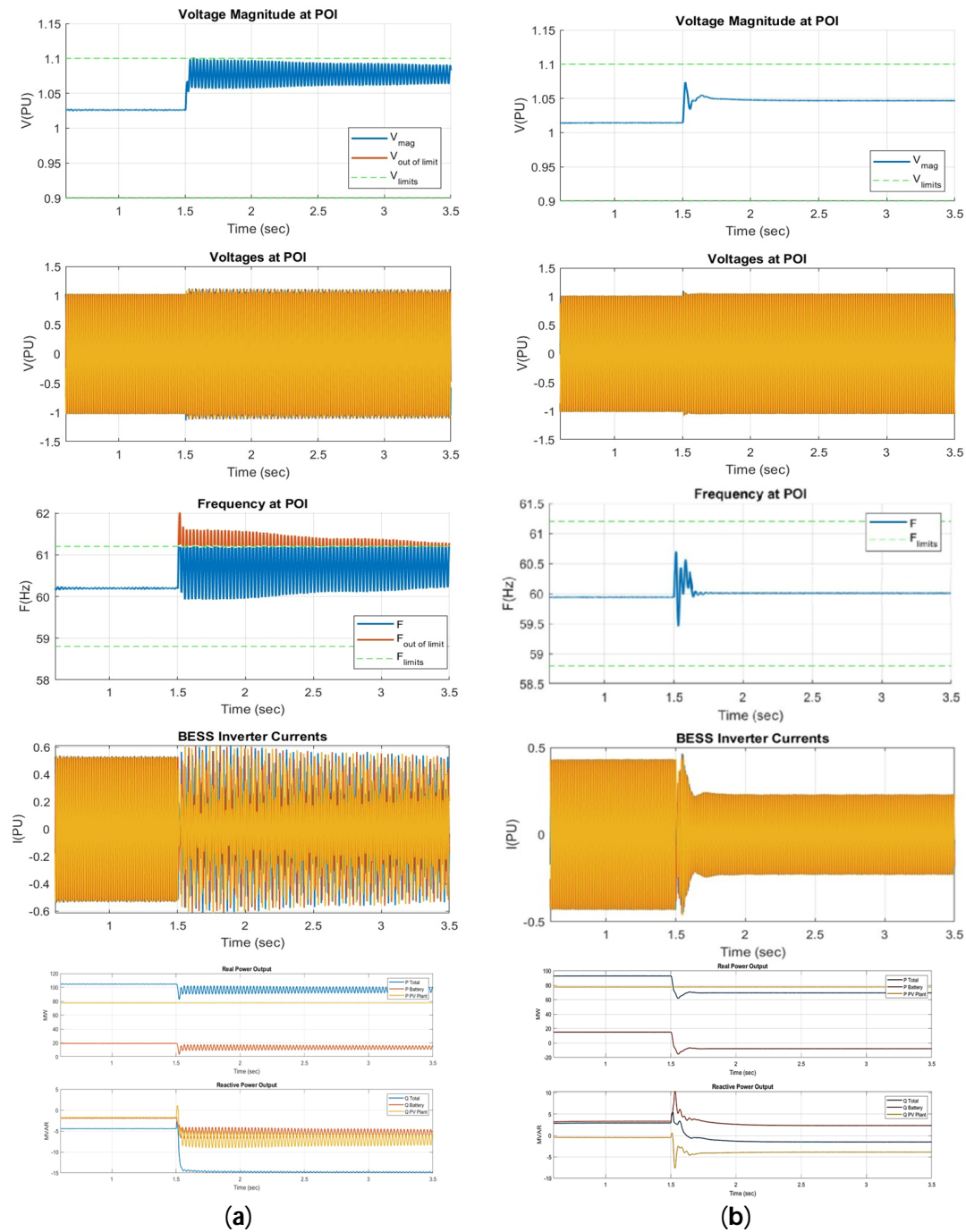


Figure 11. Performance of system parameters with (a) GFL and (b) GFM control for varying demand conditions.

Table 3. System parameters system under varying demand conditions using proposed controllers.

Parameters	Value	Switching Response (ms)
Voltage at PCC	1.05 pu	100
Frequency	60.2 Hz	200
Active power	70 MW	150
RoCoF	0.7 Hz	200
Reactive power	1.5 MVAR	150

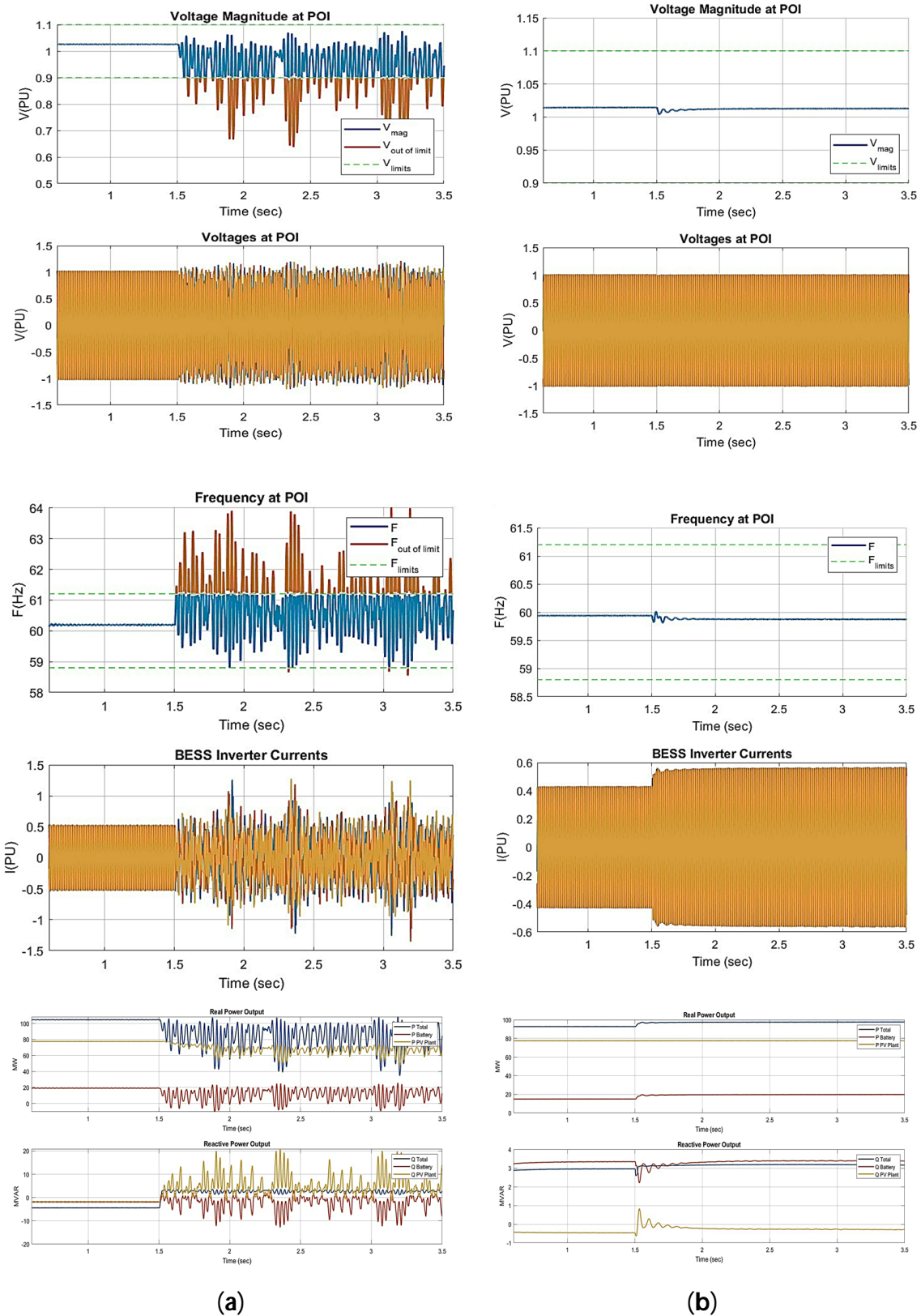


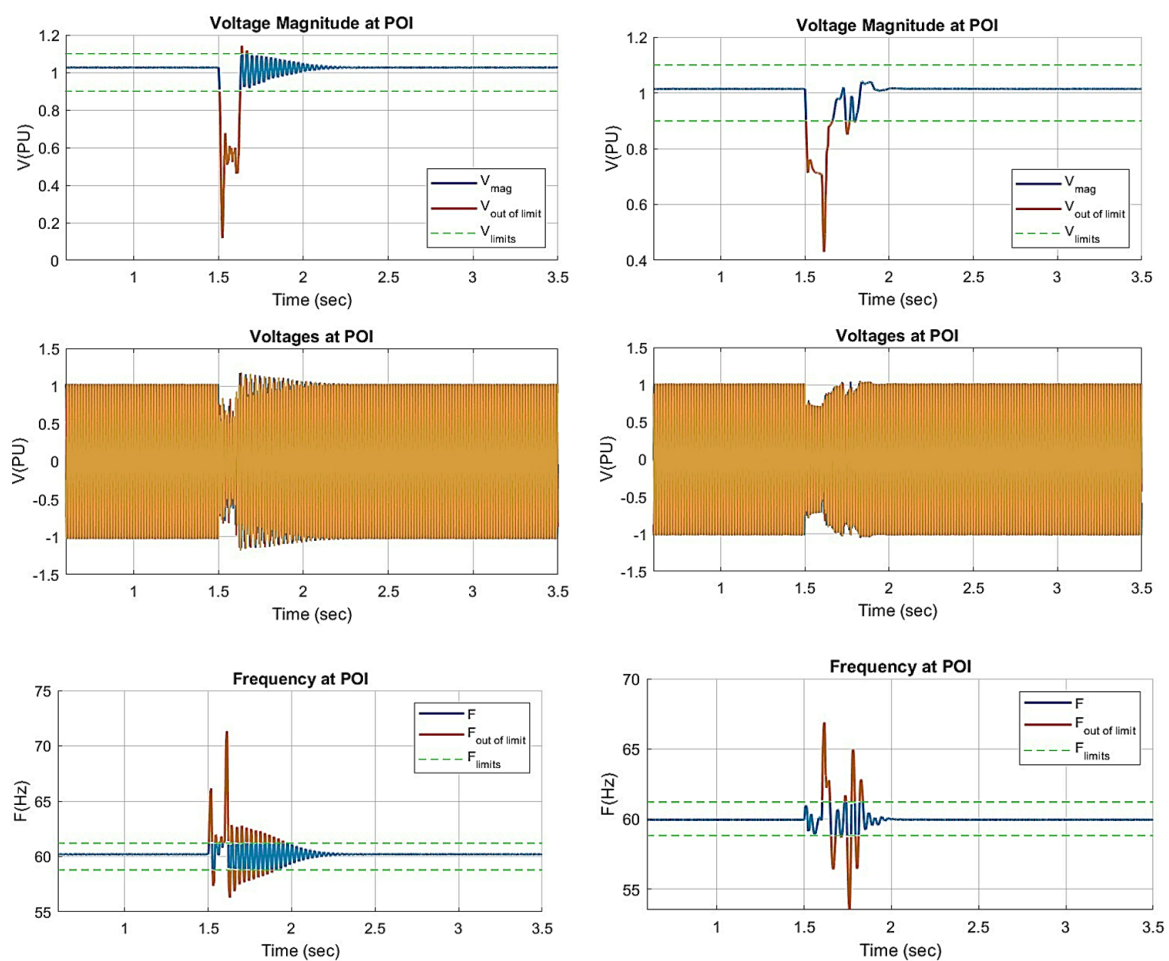
Figure 12. Performance of system parameters with (a) GFL and (b) GFM control under grid outages.

Table 4. System parameters under islanded mode of operation due to grid outages.

Parameters	Value (pu)	Switching Response (ms)
Voltage at PCC	1.02	100
Frequency	0.996	90
Inverter currents in BESS	0.58	60

Case 4: Grid faults with FRT-capable GFM inverter in grid-connected mode:

The response of the BESS unit during a three-phase symmetrical fault in the transmission line is created at 1.5 s, and the fault is cleared after 100 ms. The proposed GFM-based inverter control is provided with FRT capability by which the renewable-fed inverter is not disconnected from the grid during faults but injects controllable reactive power to support the grid. The performance of the system is compared with GFL- and GFM-based inverter control with FRT capability from the simulation results as shown in Figure 13. Table 5 provides the parameter improvement with FRT-capable GFM control. It is observed that the solar PV system and BESS are able to ride through low voltage and frequency variation during the fault, which is in compliance with the ride-through requirements according to the IEEE 2800 standard. Once the fault is cleared, the system returns to its pre-fault state within 0.5 s, which is also in compliance with the post-fault recovery requirements of the IEEE 2800 standard.

**Figure 13.** Cont.

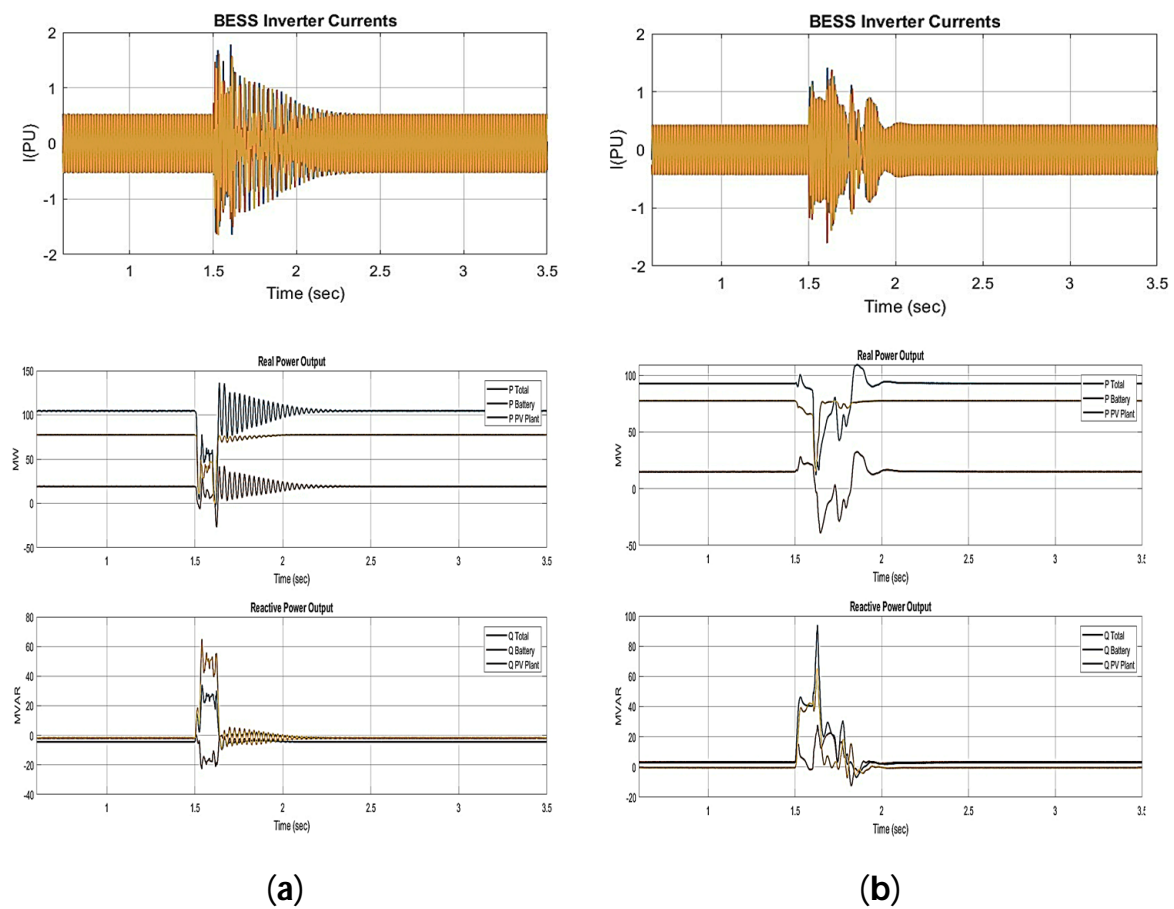


Figure 13. Performance of system parameters with (a) GFL and (b) FRT-capable GFM inverter control.

Table 5. System parameters improvement under grid faults with FRT-capable GFM inverter in grid-connected mode.

System Parameters	Percentage Improvement with FRT Capable GFL Control	Switching Response Time with GFL (s)	Percentage Improvement with FRT-Capable Proposed GFM Control	Switching Response Time with GFM (s)
System Frequency	3%	0.8	69.3%	0.3
Grid Voltage	52%	0.8	70%	0.3
Grid Current	40%	0.6	58%	0.2
Real Power	54%	0.6	81%	0.2

5. Description of Hardware Setup

This proposed GFM-based inverter control and GFL-based inverter control were implemented in a hardware setup of a 1 kW grid-tied PV-BESS microgrid network, as shown in Figure 14, and the single-line diagram of the setup is provided in Figure 15. The specifications of components in the hardware setup are provided in Table 6; the setup comprised solar PV panels, battery systems, a boost converter, FPGA processors, an inverter module, a bidirectional converter, a grid sensing module, a three-phase autotransformer and grid interfaces. The proposed controllers were deployed in FPGA SPARTAN6 processor boards. The ac- and dc-side measurements were obtained from the sensors in the grid sensing module. The ac-side measurements included voltages and current at PCC, and the dc-side measurement was voltage at the dc link acquired using a digital storage oscilloscope.

The grid fault was sensed by adjusting the isolation transformer to create a dip and rise in grid voltage, thereby realizing the low-voltage and high-voltage conditions.

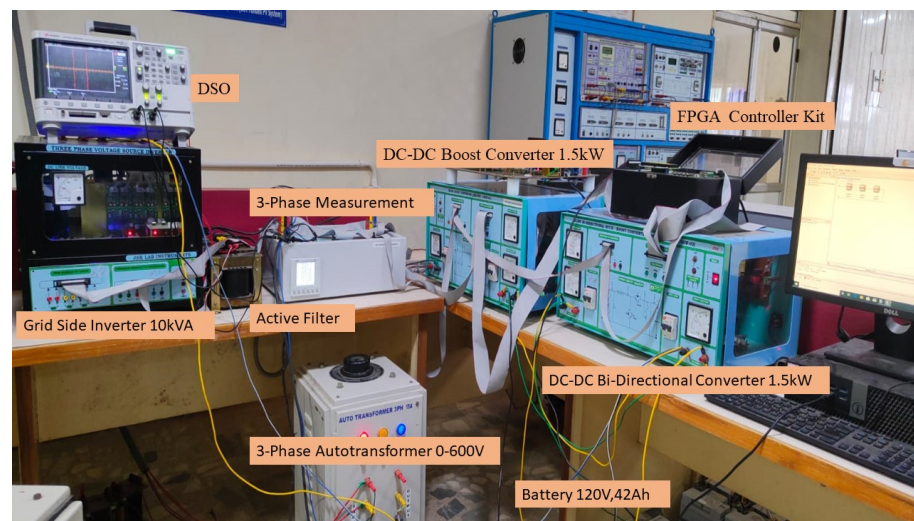


Figure 14. Microgrid setup with solar PV-BESS integrated with grid.

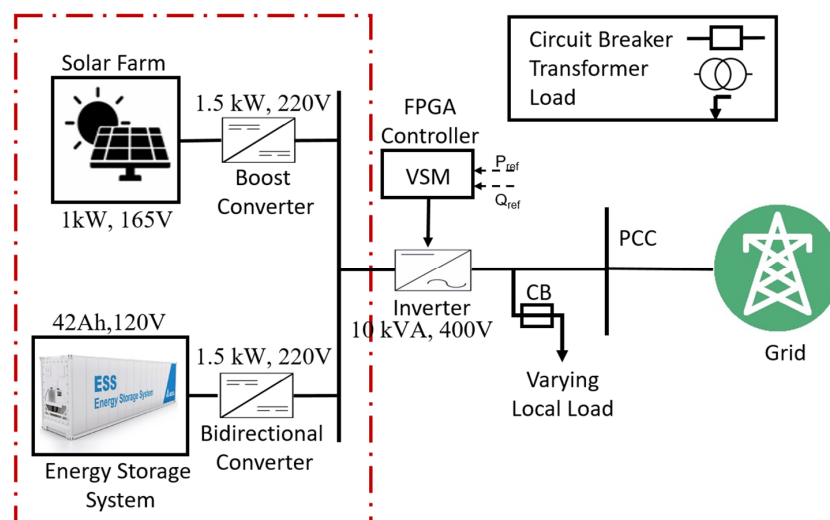


Figure 15. Single-line diagram of hardware setup.

Table 6. Specifications of microgrid hardware setup.

Components	Ratings
PV Rating	1 KW
System Line Voltage	400 V
Frequency	50 Hz
DC-Link Voltage	220 V
Inverter Rating	10 kVA, 400 V, 10 A
Inverter Switching Frequency	10 kHz
DC-DC Boost Converter Rating	1.5 kW, 400 V
Boost Converter Switching Frequency	5–20 kHz
Inverter Output Filter Inductance	5 mH, 25 A
Inverter Output Filter Capacitance	4 uF, 440 V AC

6. Discussion of Experimental Setup

The proposed control algorithm for GFL- and GFM-based inverters in a microgrid hardware setup comprising solar PV and battery systems was implemented in FPGA-based processor boards. The proposed algorithms were tested under grid and islanded modes of operation. The algorithms were also tested under varying solar irradiation, varying demand and both varying irradiance and demand conditions. The comparison of GFL- and GFM-based inverter controls in the hardware setup was implemented and analyzed using the system parameters.

Case 1: GFL- and GFM-based inverter control in grid-connected operation

When the microgrid comprising solar PV and battery systems is operated in grid-connected mode, the generated power from renewables and storage systems is fed into the grid. Figure 16 displays the experimental results of GFL and GFM control under grid-connected operation. When the system is subjected to varying solar irradiance conditions and is implemented with the proposed control models, it is found that GFM has minimum switching transients when compared to GFL control during grid-connected operation. The real power and reactive power have fewer oscillations in GFM than in GFL control. The real and reactive power injected into the grid is more stabilized in GFM-based control when integrated with the grid. Figure 17 displays the performance of boost and bidirectional converters of the solar PV system and BESS in a microgrid network. Table 7 provides the performance of the microgrid experimental setup in grid-connected operation. As the GFM-based inverter control does not require stiff and stable voltage at the PCC, the microgrid network with GFM-based inverter control can exhibit more real power penetration than the conventional GFL inverter control. It is understood from the experimental results that GFM control can provide a faster response than GFL control as GFM control can stabilize the grid conditions instantaneously.

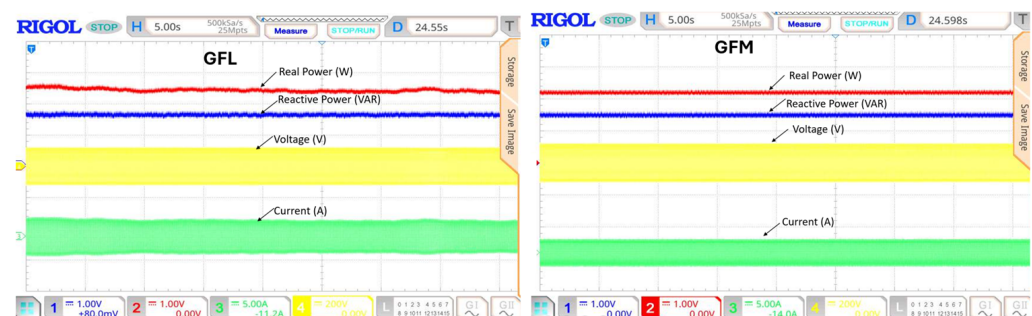


Figure 16. Performance of system under varying solar irradiation in grid-connected operation.

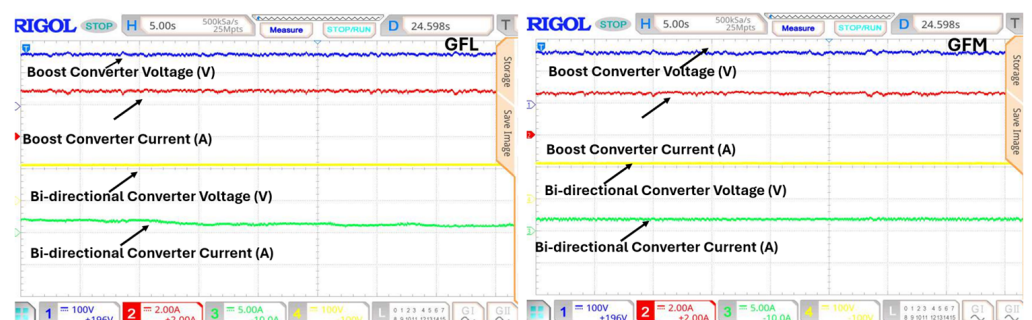


Figure 17. Performance of boost and bidirectional converters of the solar PV system and BESS in a microgrid network.

Table 7. Parameters of hardware setup under grid-connected operation.

Mode	GFL-Based Inverter Control	GFM-Based Inverter Control
Voltage at PCC	81.8 V	82.3 V
Voltage at DC link	243 V	244 V
Active power	616 W	618 W
Reactive power	26 VAR	20 VAR

Case 2: GFL and GFM based inverter control in islanded operation

The integrated GFL- and GFM-based inverter controls were implemented in FPGA-based controller boards in a real-time microgrid setup. When the network is switched to islanded operational mode in which the local renewable generations and load are available, the renewable-fed inverter is operated in grid-forming control by which voltage and frequency are regulated. The hardware setup was tested under islanded operation by disconnecting the grid and retaining only solar PV, BESS and local load. The system was analyzed under two cases, namely varying irradiance conditions and varying irradiance and load conditions, and the experimental results are provided in Figures 18 and 19, respectively. Table 8 depicts the performance of the system under GFM- and GFL-based inverter controls. The performance of the system clearly demonstrates that more oscillations and a longer settling time are observed in the GFL inverter control when compared with GFM inverter control. GFM-based inverter control provides a fast system response when subjected to varying irradiance and loading conditions.

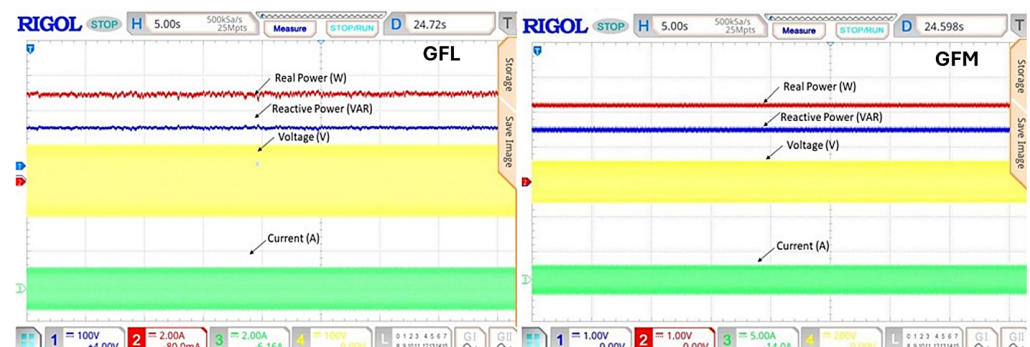
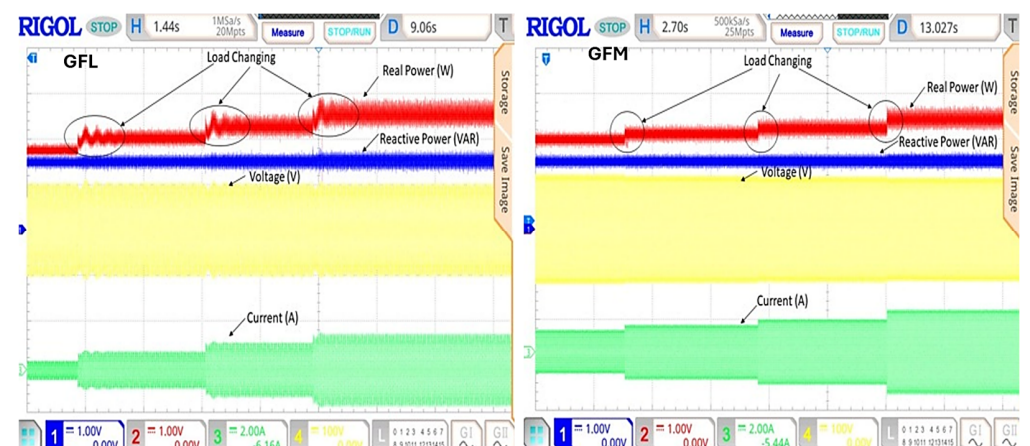
**Figure 18.** Performance of experimental setup under varying irradiance in islanded mode of operation.**Figure 19.** Performance of experimental setup under varying irradiance and loading conditions in islanded mode of operation.

Table 8. Parameters of hardware setup under islanded operation.

Mode		GFL		GFM	
Parameters	Value	Switching Response (ms)	Value	Switching Response (ms)	
Voltage at PCC	57.9 V	5 ms	65 V	0.3 ms	
Voltage at DC link	243 V	5 ms	244 V	0.3 ms	
Active power	263 W	4 ms	331 W	0.2 ms	
Reactive power	0	5 ms	0	0.3 ms	

7. Conclusions and Future Scope

In this work, grid-forming inverter-based control is developed and implemented in a solar PV system- and BESS-integrated microgrid network. The proposed model is tested under different operating conditions: varying solar irradiation, varying demand conditions, islanded mode and grid faults. The GFM-based inverter control provides an immediate response to the system and reduces switching transients, maintaining the reliability and stability of the system. The FRT capability is incorporated in the control of GFL and GFM inverters, and the system performances are compared. It is understood from the results under different test conditions that GFM control offers increased voltage and frequency stability. The proposed control strategy for renewable-fed inverters achieves a lower rate of change of frequency under system disturbances. The GFM-based inverter control achieves a reduced current limit, and the steady state is achieved quickly, which leads to increased fault-clearing time. In the future works, the authors will concentrate on the development of implementing soft computing approaches for GFM-based inverter control. The GFM-based inverter control will be studied in terms of the transient and small signal stability of the system.

Author Contributions: All authors contributed equally to the manuscript. All authors have read and agreed to the published version of the manuscript.

Funding: This research received no external funding.

Data Availability Statement: Data are contained within the article.

Conflicts of Interest: The authors declare no conflict of interest.

References

1. Fang, J.; Li, H.; Tang, Y.; Blaabjerg, F. Distributed Power System Virtual Inertia Implemented by Grid-Connected Power Converters. *IEEE Trans. Power Electron.* **2018**, *33*, 8488–8499. [\[CrossRef\]](#)
2. Peng, Q.; Jiang, Q.; Yang, Y.; Liu, T.; Wang, H.; Blaabjerg, F. On the Stability of Power Electronics-Dominated Systems: Challenges and Potential Solutions. *IEEE Trans. Ind. Appl.* **2019**, *55*, 7657–7670. [\[CrossRef\]](#)
3. Rosso, R.; Wang, X.; Liserre, M.; Lu, X.; Engelken, S. Grid-Forming Converters: Control Approaches, Grid-Synchronization, and Future Trends—A Review. *IEEE Open J. Ind. Appl.* **2021**, *2*, 93–109. [\[CrossRef\]](#)
4. Mittal, R.; Miao, Z. Analytical Model of A Grid-Forming Inverter. In Proceedings of the 2022 IEEE Power & Energy Society General Meeting (PESGM), Denver, CO, USA, 17–21 July 2022; pp. 1–5.
5. Smith, J.W.; Sunderman, W.; Dugan, R.; Seal, B. Smart inverter volt/var control functions for high penetration of PV on distribution systems. In Proceedings of the 2011 IEEE/PES Power Systems Conference and Exposition, Phoenix, AZ, USA, 20–23 March 2011; pp. 1–6.
6. Kikusato, H.; Ustun, T.S.; Hashimoto, J.; Otani, K.; Nagakura, T.; Yoshioka, Y.; Maeda, R.; Mori, K. Developing Power Hardware-in-the-Loop Based Testing Environment for Volt-Var and Frequency-Watt Functions of 500 kW Photovoltaic Smart Inverter. *IEEE Access* **2020**, *8*, 224135–224144. [\[CrossRef\]](#)
7. *IEEE Std 1547-2018*; IEEE Standard for Interconnection and Interoperability of Distributed Energy Resources with Associated Electric Power Systems Interfaces. IEEE: Piscataway, NJ, USA, 2018.
8. *EN 50549-1*; Requirements for Generating Plants to be Connected in Parallel with Distribution Networks—Part 1: Connection to a LV Distribution Network—Generating Plants Up to and Including Type B. European Committee for Standardization: Brussels, Belgium, 2019.

9. EN 50549-2; Requirements for Generating Plants to be Connected in Parallel with Distribution Networks—Part 2: Connection to a MV Distribution Network—Generating Plants Up to and Including Type B. European Committee for Standardization: Brussels, Belgium, 2019.
10. Hoke, A.; Giraldez, J.; Palmintier, B.; Ifuku, E.; Asano, M.; Ueda, R.; Symko-Davies, M. Setting the smart solar standard: Collaborations between hawaiian electric and the national renewable energy laboratory. *IEEE Power Energy Mag.* **2018**, *16*, 18–29. [\[CrossRef\]](#)
11. Lasseter, R.H.; Chen, Z.; Pattabiraman, D. Grid-Forming Inverters: A Critical Asset for the Power Grid. *IEEE J. Emerg. Sel. Top. Power Electron.* **2020**, *8*, 925–935. [\[CrossRef\]](#)
12. Yazdani, A.; Iravani, R. *Voltage-Sourced Converters in Power Systems: Modeling, Control, and Applications*; IEEE: Piscataway, NJ, USA, 2010; pp. i–xix. ISBN 9780470551561.
13. Rocabert, A.L.; Blaabjerg, F.; Rodríguez, P. Control of power converters in ac microgrids. *IEEE Trans. Power Electron.* **2012**, *27*, 4734–4749. [\[CrossRef\]](#)
14. Pattabiraman, D.; Lasseter, R.; Jahns, T. Comparison of Grid Following and Grid Forming Control for a High Inverter Penetration Power System. In Proceedings of the 2018 IEEE Power & Energy Society General Meeting (PESGM), Portland, OR, USA, 5–10 August 2018; pp. 1–5. [\[CrossRef\]](#)
15. Zuo, Y.; Yuan, Z.; Sossan, F.; Zecchino, A.; Cherkaoui, R.; Paolone, M. Performance assessment of grid-forming and grid-following converter-interfaced battery energy storage systems on frequency regulation in low-inertia power grids. *Sustain. Energy Grids Netw.* **2021**, *27*, 100496. [\[CrossRef\]](#)
16. Li, Y.; Gu, Y.; Green, T.C. Revisiting grid-forming and grid-following inverters: A duality theory. *IEEE Trans. Power Syst.* **2022**, *37*, 4541–4554. [\[CrossRef\]](#)
17. Orihara, D.; Kikusato, H.; Hashimoto, J.; Otani, K.; Takamatsu, T.; Oozeki, T.; Taoka, H.; Matsuura, T.; Miyazaki, S.; Hamada, H.; et al. Contribution of Voltage Support Function to Virtual Inertia Control Performance of Inverter-Based Resource in Frequency Stability. *Energies* **2021**, *14*, 4220. [\[CrossRef\]](#)
18. Driesen, J.; Visscher, K. Virtual synchronous generators. In Proceedings of the IEEE Power Energy Society General Meeting—Conversion and Delivery of Electrical Energy in the 21st Century, Pittsburgh, PA, USA, 20–24 July 2008; pp. 1–3.
19. Ward, L.; Subburaj, A.; Demir, A.; Chamana, M.; Bayne, S.B. Analysis of Grid-Forming Inverter Controls for Grid-Connected and Islanded Microgrid Integration. *Sustainability* **2024**, *16*, 2148. [\[CrossRef\]](#)
20. Mohammed, N.; Udawatte, H.; Zhou, W.; Hill, D.J.; Bahrani, B. Grid-Forming Inverters: A Comparative Study of Different Control Strategies in Frequency and Time Domains. *IEEE Open J. Ind. Electron. Soc.* **2024**, *5*, 185–214. [\[CrossRef\]](#)
21. Wang, B.; Burgos, R.; Wen, B. Grid-Forming Inverter Control Strategy with Improved Fault Ride Through Capability. In Proceedings of the 2022 IEEE Energy Conversion Congress and Exposition (ECCE), Detroit, MI, USA, 9–13 October 2022; pp. 1–8.
22. Lin, Y.; Eto, J.H.; Johnson, B.B.; Flicker, J.D.; Lasseter, R.H.; Villegas Pico, H.N.; Seo, G.S.; Pierre, B.J.; Ellis, A. *Research Roadmap on Grid-Forming Inverters*; Technical Report; National Renewable Energy Laboratory (NREL): Golden, CO, USA, 2020.
23. Tabassum, T.; Toker, O.; Khalghani, M.R. Cyber-physical anomaly detection for inverter-based microgrid using autoencoder neural network. *Appl. Energy* **2024**, *355*, 122283. [\[CrossRef\]](#)
24. Ahmad, S.; Shafiullah, M.; Ahmed, C.B.; Alowaiifeer, M. A Review of Microgrid Energy Management and Control Strategies. *IEEE Access* **2023**, *11*, 21729–21757. [\[CrossRef\]](#)
25. Van, L.P.; Chi, K.D.; Duc, T.N. Review of hydrogen technologies based microgrid: Energy management systems, challenges and future recommendations. *Int. J. Hydrog. Energy* **2023**, *48*, 14127–14148. [\[CrossRef\]](#)
26. González, I.; Calderón, A.J.; Folgado, F.J. IoT real time system for monitoring lithium-ion battery long-term operation in microgrids. *J. Energy Storage* **2022**, *51*, 104596. [\[CrossRef\]](#)
27. Davi, M.J.; Oleskovicz, M.; Lopes, F.V. Study on IEEE 2800–2022 standard benefits for transmission line protection in the presence of inverter-based resources. *Electr. Power Syst. Res.* **2023**, *220*, 109304. [\[CrossRef\]](#)

Disclaimer/Publisher’s Note: The statements, opinions and data contained in all publications are solely those of the individual author(s) and contributor(s) and not of MDPI and/or the editor(s). MDPI and/or the editor(s) disclaim responsibility for any injury to people or property resulting from any ideas, methods, instructions or products referred to in the content.